Letter to the Editors

Raman spectra of tetragonal zirconia: powder to zircaloy oxide frequency shift

Pierre Barbéris [a], Gaëlle Corolleur-Thomas [b], René Guinebretière [c], Thérèse Merle-Mejean [b], Andrei Mirgorodsky [b], Pierre Quintard [b,*]

[a] *CEZUS, Direction des Recherches et Développements, Centre de Recherches d'Ugine, Ugine cedex F-73403, France*
[b] *Laboratoire de Science des Procédes Céramiques (SPCTS), UMR 6638 du CNRS, Faculté des Sciences, 123 ave A. Thomas, Limoges F-87060, France*
[c] *Laboratoire de Science des Procédes Céramiques (SPCTS), UMR 6638 du CNRS, École Nationale Supérieure de Céramiques Industrielles (ENSCI), 47 ave A. Thomas, Limoges F-87065, France*

Abstract

The shifts of the two main characteristic Raman active bands of t-ZrO$_2$ in oxide films developed on zirconium alloy relatively to their position in nanopowder (267, 456 cm^{-1}) are discussed. The origin of the shifts is analyzed within the lattice dynamical treatment according to which neither hydrostatic compression nor biaxial one can be responsible for this shift. It is put in evidence that only an abnormal high value of the internal tetragonality ($\Delta z = L_z/c$) can provide this effect. Additionally, the symmetry assignment of the two bands are determined which, in particular, argues for the identification of the band near 267 cm^{-1} as a totally symmetric A_{1g} soft mode. © 2001 Elsevier Science B.V. All rights reserved.

1. Introduction

It was displayed in a previous paper [1] that the Raman scattering of tetragonal zirconia developed as oxide films at 680 K in steam (autoclave) on Zircaloy 4 shows systematic shifts of the main characteristic bands relatively to their positions in the powder sample spectra. Compared to those of a pure tetragonal nanopowder, these main bands with strong intensities at 267 and 456 cm^{-1} were shifted by +15 and −13 cm^{-1}, respectively. Analogous observations on Zr–Nb alloy oxide films have been reported by Lin [2,3]. The monoclinic zirconia peaks were almost unchanged in position.

The purpose of this paper is to give some explanations for these remarkable effects which could be related [1] neither to additive elements (chemical alloying) nor to any known high-pressure phase. Using the CRYME code [4] capable in particular of calculating the stress-induced variations in the spectra, we have modeled and analyzed the behaviors of the Raman spectra as a function of isotropic and biaxial stresses and of the $L_z = \Delta z/c$ displacement of the oxygen atom from its position in the cubic phase.

The interatomic potentials were approximated by the rigid ion model (RIM) which included coulombic forces and non-coulombic repulsive ones. The coulombic interactions were described via the effective charge of O and Zr atoms respectively equal to −1.185e and +2.370e. The parameters A and B (second and first derivatives of $V_{(r)}$) of the non-coulombic interaction as a function of interatomic distances for O–O and Zr–O bond lengths are presented in Fig. 1. The relevant analytic expressions for the non-coulombic energy $V_{(r)}$ were given in [5]. These interatomic potentials have previously given realistic reproduction of Raman spectra of m-, t-, c- and o-zirconia thus manifesting their *transferability*.

2. Crystal parameters for the t-ZrO$_2$

First of all we had to determine the possible crystal structure of pure t-ZrO$_2$ at room temperature (RT). After the first determination by Teufer [6], Aldebert and

---

* Corresponding author.
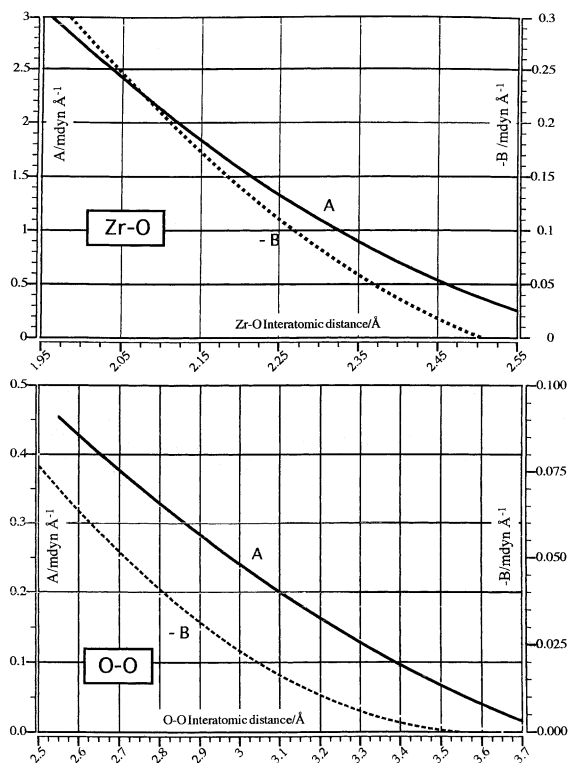*E-mail address:* quintard@unilim.fr (P. Quintard).

Fig. 1. First and second order force constants (dotted and bold curves, respectively) of the short range interatomic potential of the non-coulombic interactions, as the function of interatomic distances, for O–O and Zr–O bond lengths. 1 mdyn $\text{Å}^{-1} = 1 \text{ N cm}^{-1}$. These values of *transferable* RIM interatomic potentials have previously given realistic reproduction of Raman spectra of m-, t-, c- and o-zirconia.
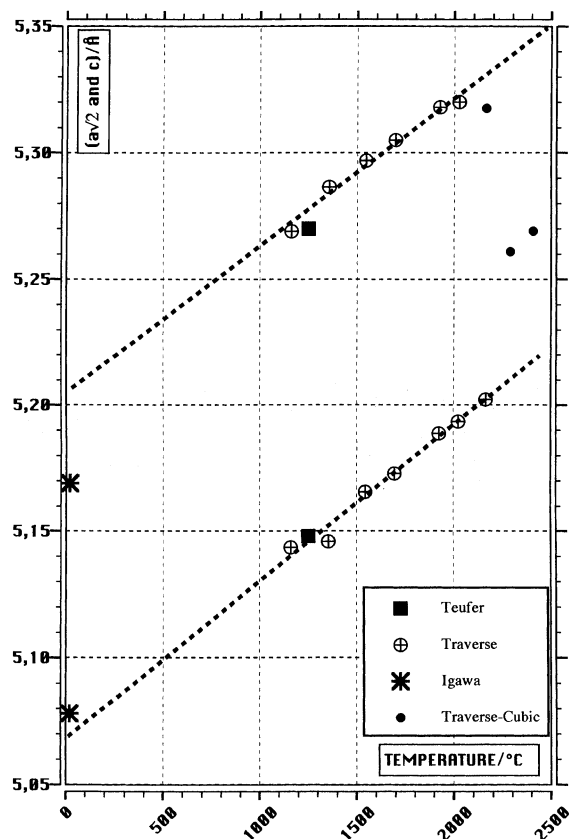

Fig. 2. Linear extrapolation at RT of the high temperature structures given in [7] (Traverse) and that obtained at RT from nano-powders in [8] (Igawa).

Traverse [7] gave the crystal structure of tetragonal zirconia at temperatures higher than 1500 K up to the t–c transformation. It is well-known that this t-phase can be stabilized at RT either by different additives or through a nanometric size. The extrapolation of the cell parameters and Δz values, to RT from high temperature structures, are given in Fig. 2 and Fig. 3, respectively. The results are summarized as crystal PQ1 in Table 1. The high temperature structure just above the t–m transition [7] is named PQ3.

A size-stabilized RT structure (PQ2) of a nanopowder was given by Igawa [8]; it was prepared from alkoxide precursor and annealed at 670 K. Another one, described by Djurado et al. [9], was obtained by a spray-pyrolisis method (PQ4). A systematic study of the evolution of the structure of xerogels-, aerogels- and precipitated-t-ZrO$_2$ [10] showed that the c, a and Δz values for a given process were sensitive to annealing temperature and accompanying a grain growth. An accurate direct measurement of Δz is difficult and could only be reached using neutrons diffraction. In the range 770–1170 K, the c and c/a values can change by about 0.4% and 0.5%, respectively, while

Δz variation could be about 10–20%. Typically Δz can vary from 0.040 to 0.050. Thus PQ1, PQ2 and PQ4 model crystals (Table 1) have the same probability to represent the real structure of a size-stabilized tetragonal phase, and the structure given in [8] would be slightly different if the nanometric powder had been annealed at higher temperature. The oxygen positions calculated according to a relationship between Δz and tetragonality c/a: $\Delta z = 0.24\sqrt{(1 - a^2/c^2)}$ [11] are also presented in Table 1. The different c, a and Δz values of crystals PQ2, PQ4 (so as low additive stabilized ones) give similar frequencies of the characteristic peaks.

The four crystal structures retained in Table 1 for further calculations, are also in good agreement with those extrapolated to 0% molar fraction additive of:
Y$_2$O$_3$:
$a\sqrt{2} = 5.080$ Å, $c = 5.194$ Å, $c/a = 1.022$ [12],
$a\sqrt{2} = 5.086$ Å, $c = 5.189$ Å, $c/a = 1.0203$ [13],
CeO$_2$:
$a\sqrt{2} = 5.0821$, $c = 5.1855$, $c/a = 1.0203$ [14,15].
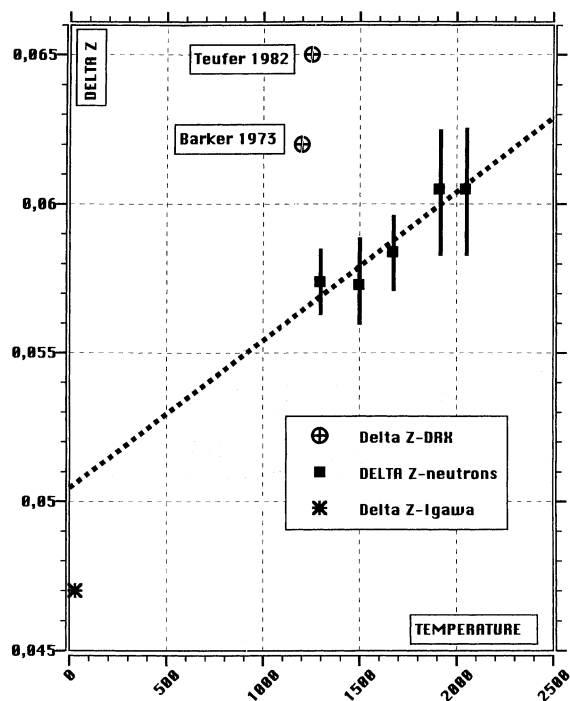We can conclude that these four structures have to be checked for the simulation, whereas the results for PQ3

Fig. 3. Linear extrapolation at RT of the high temperature results on Δz [7] and that obtained at RT from nano-powders [8]. The correlation coefficient (r^2) is 0.90 for the extrapolation; the accuracy domain for [8] is 0.047 ± 0.003.

could possibly diverge from the common results, because it is too far from a realistic representation of a RT tetragonal phase.

3. Behavior of a tetragonal structure under isotropic stress and related frequency shifts

Our first hypothesis was that the shift under consideration appears because of an isotropic compressive stress which can arise in the t-ZrO$_2$ structure. Actually, a biaxial stress in the (x,y) plane of a few GPa was found at the metal/oxide (t-ZrO$_2$) interface [16,17]; additionally, due to the t–m transformation in the upper layer of the oxide film, a compressive force along z can also appear because of a 4% volume increase. It is not, therefore, meaningful to consider a three-axial stress as the cause of the frequency shifts in question. So we modeled the behavior of the different crystal structures retained, under an isotropic stress of typically 3 GPa. For other stresses around this value, results could be obtained through a linear extension.

From the compressibilities of a and c cell parameters, directly calculated by CRYME from the interatomic potentials (Table 2), we can estimate these parameters for a lattice stressed by 3 GPa. The Δz value is then determined as resulting from the relaxation of the structure. All the model crystals showed an isotropic compressive stress-induced decrease of Δz, in parallel to that of a and c (Tables 1 and 2), giving notice of a lowering of tetragonality, so that a/c is expected to be nearly unity (i.e., cubic) for $\sim$40 GPa.

For the most realistic RT structures (PQ 1, 2, 4), the a, c and Δz parameters have decreased by 0.5%, 0.8% and 10%, respectively, due to this stress of 3 GPa. In the range 0–10 GPa, the $\partial(\Delta z)/\partial P$ slope is equal to -0.00139 GPa^{-1} for PQ2 crystal. The absolute distance L_z (0.23–0.27 Å, Table 1) is decreased by 0.0072 Å for 1 GPa. The results are summarized in Table 2. The $\partial(\Delta z)/\partial P$ slope value reduces at increasing pressure due to the decreasing compressibility of the stressed lattices and stiffening of Zr–O bonds. We determined the slope values as -0.00113, -0.00072 and -0.00017 GPa^{-1} for PQ2 stressed at 10, 20 and 30 GPa, respectively.

The calculated frequency shifts are close to that observed under hydrostatic compression [18] but quite different from the results of the simulation in our previous work [1] in which the use of a valence force field (VFF) taken from [19] laid an incorrect asymptotic limit for the stiffness of bonds shorter than 2.08 Å. Conse-

Table 1

Crystal parameters used for tetragonal zirconia in our lattice dynamical calculation (see Section 2)[a]

Crystal	$a = b$/Å	c/Å	$c/a\sqrt{2}$	Δz exp.	Δz calc.	Zr–O/Å	L_z/Å	Remarks and reference
PQ1	3.5836	5.2050	1.027	0.051	0.055	I: 2.0696	0.2658	RT from High Temperature [6,7]
						II: 2.3801		
PQ2	3.592	5.170	1.018	0.047	0.045	I: 2.0802	0.2430	Nanometric RT [8]
						II: 2.3629		
PQ3	3.637	5.2689	1.024	0.065	0.052	I: 2.0633	0.3425	High Temperature 1500 K [6]
						II: 2.4620		
PQ4	3.596	5.187	1.020	0.045	0.048	I: 2.0899	0.2334	Nanometric, RT [9]
						II: 2.3610		

[a] Δz experimental (exp.) was taken from the reference in the last column, Δz was calculated (calc.) using the formula in [11].

Table 2
Shifts of the 267 and 456 cm^{-1} modes under an *isotropic* stress of 3 Gpa[a]

Crystal	Linear compressibility GPa^{-1} 10^3	Δz	Shift/cm^{-1} from 267 cm^{-1}	Shift/cm^{-1} from 456 cm^{-1}	$\partial(\Delta z)/\partial P$/GPa^{-1}
PQ1	a: 1.55 c: 2. 69	0.0468	−10.7	+11.1	−0.00151
PQ2	a: 1.53 c: 2.49	0.0428	−8.7	+13.8	−0.00139
PQ3	a: 1.94 c: 3.98	0.0581	−9.4	+19.7	−0.0023
PQ4	a: 1.57 c: 2.56	0.0406	−9.4	+14.0	−0.00147

[a] $\Delta z = L_z/c$ is given after relaxation of the structure. The compressibility is given for *a* and *c* lattice parameters (e.g., 0.00155 GPa^{-1}).

quently these values for the short Zr–O1 (Table 1) bonds were overestimated.

Our results (Table 2) clearly disclose that the calculated isotropic stress-induced shifts of the 267 and 456 cm^{-1} frequencies are opposite to the experimental shifts [1] (see Section 1), i.e., such a compressive stress cannot explain the observed phenomenon and a tensile stress (i.e., a negative pressure) would be necessary but this is not consistent with [16,17].

4. Behavior of a tetragonal structure under biaxial stress and associated frequency shifts

In this part we will consider the frequency shifts produced by a typical $P = 3$ GPa biaxial (x, y) compressive stress of the primitive cell. The oxide film is highly textured [20] with *c* axis perpendicular to the interface so that the stress acts in the plane $\{1\,1\,0\}$ containing *a* and *b* axis. This stress would induce a lengthening (Δc) of the *c* edge perpendicular to the surface of zircaloy. The Δc extension is related to the $\Delta a = \Delta b$ variation as: $\Delta c/c = -(\Delta a/a)(2C_{13}/C_{33})$ where the C_{ij} are the elastic constants. Typically, in the calculation for PQ2, C_{13} is equal to 55 GPa and C_{33} to 335 GPa, as estimated by our model. The relaxation of $\Delta z(= L_z/c)$ is obtained using the relation previously used in [21], *U* being the homogeneous strain

$$\partial L_z/\partial P = \Sigma(\partial L_z/\partial U_i)(\partial U_i/\partial P).$$

As an example, for a stress of 3 GPa applied on *a* and *b*, we obtained for the PQ2 crystal, ΔL_z equals to −0.00306 Å. This means that the relaxed Δz is, now, for this crystal equal to 0.0464 instead of the initial value of 0.0470. These results are reported in Table 3. The $a = b$ and *c* parameters changed by −0.5% and +0.2%, respectively, and the related Δz value allowed us to construct a new PQ2 biaxially stressed crystal. By applying the RIM potential, we could estimate the shifts of the bands in question. In this condition, $\partial(\Delta z)/\partial P$ is always negative. It is worth noticing that the slope value, −0.0002 GPa^{-1},

Table 3
Shifts of the characteristic frequencies under a *biaxial* (a, b) stress of 3 Gpa[a]

Crystal	Δz shift	267 cm^{-1} shift	458 cm^{-1} shift
PQ1	0.0504	+1.3	+5.2
PQ2	0.0464	+1.2	+5.4
PQ3	0.0636	+1.9	+6.9
PQ4	0.0444	+1.1	+5.5

[a] Δz is given after relaxation of the structure.

is very little, compared to the case of the isotropic compression (see Section 3), and it induces the low sensitivity of the shifts to the biaxial stress.

The results of our calculations (assigned in [22,23]) are given on Table 3. The calculated shifts are far from the observed values (see Section 1) and, moreover, the sign of the 456 cm^{-1} band shift contradicts the observed one. This leads to the conclusion that a biaxial stress of a few GPa cannot explain the experimental evidence [1].

5. Shifts of t-ZrO$_2$ Raman frequencies under Δz variations

The above results fail to explain the observed effects of the frequency shifts of the two vibrations whose positions in powder samples are located near 267 and 456 cm^{-1}. However, the detailed analysis of these results allows us to conclude that this is the Δz value (the factor of internal tetragonality of t-ZrO$_2$ lattice) which, practically, completely dominates the behavior of the vibrational frequencies of the t-ZrO$_2$ lattice.

Therefore, presently, we focus our attention on this factor. First, the behaviors of the two above mentioned vibrations were studied as a function of the Δz values. Variations of ±8% of this parameter relatively to its magnitudes in the model structures of t-ZrO$_2$ were investigated. Such a Δz variation directly influence the Zr–O bond lengths which quite linearly vary with Δz (Fig. 4). The results of our calculations are reported in Fig. 5 well reproducing at one and the same time, the sign and the
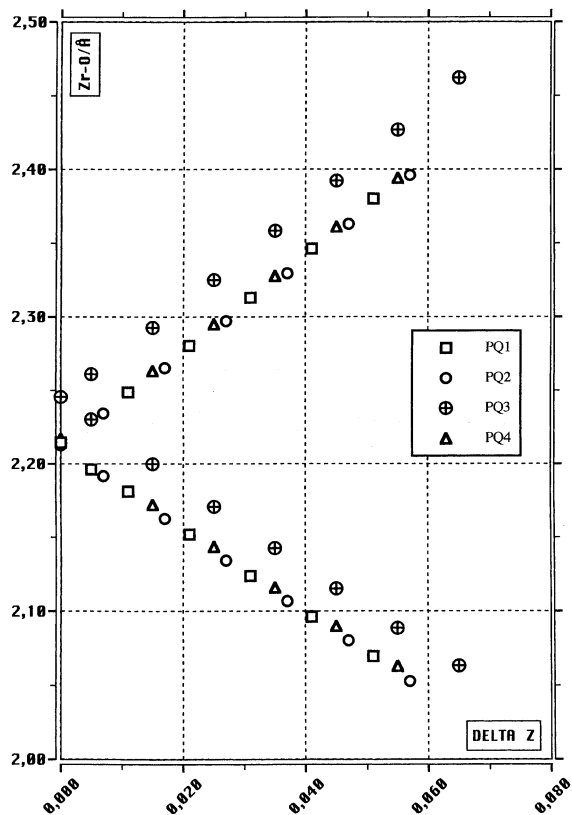
Fig. 4. Evolution of short (I) and long (II) Zr–O bond lengths with Δz for the different crystals. PQ1, PQ2, PQ4 have similar behavior. The high temperature PQ3 crystal diverges from the three others due to thermal expansion of bond lengths.

Fig. 5. Evolution of the 267 and 456 cm^{-1} frequencies versus $\Delta z = L_z/c$, around the nominal Δz value. Signification of A_{1g} and E_g representation is discussed in the text. With Δz increase A_{1g} frequencies (≈ 267 cm^{-1}) [22–24] are increased and E_g frequencies (≈ 456 cm^{-1}) are lowered according to, respectively, an hardening and softening of these modes.

magnitude of the observed shifts; as an example, in the PQ2 crystal, the origin of shifts of $+15$ cm^{-1} for the phonon near 267 and -13 cm^{-1} for the phonon near 456 cm^{-1} are explained by the increase of Δz from 0.047 (in the nanopowder sample, Table 1) to 0.055 (in the massive oxide).

In Figs. 5 and 6, we followed the A_{1g} assignment for the strongest Raman active line near 267 cm^{-1} experimentally established by Sobol et al. [24]. It is based on polarized Raman spectra of a single crystal of stabilized tetragonal zirconia. Using this assignment as a basic experimental evidence, the lattice-dynamical model treatments [22,23,25,26] were capable of physically consistently explaining both elastic and vibrational properties of ZrO$_2$ in the cubic, tetragonal, monoclinic and orthorhombic phases.

For all the crystals, the behaviors of both phonons show the same effect: the frequency related to the experimentally observed band near 456 cm^{-1} always drops at increasing Δz values; whereas, at the same time, the frequency of the phonon observed near 267 cm^{-1} always increases. Thus, the physical reason for both experi-
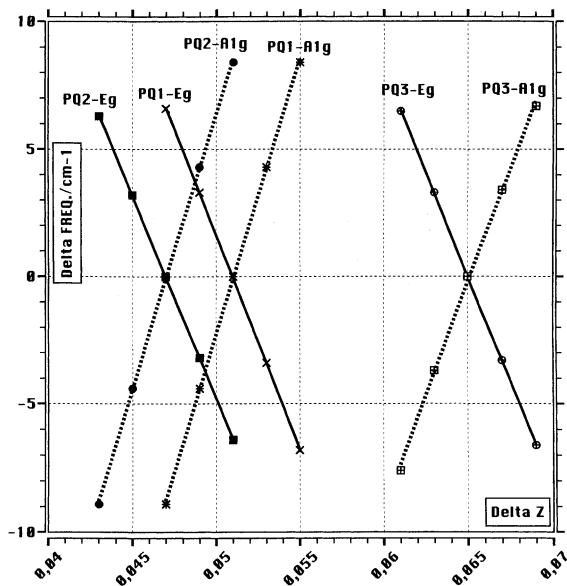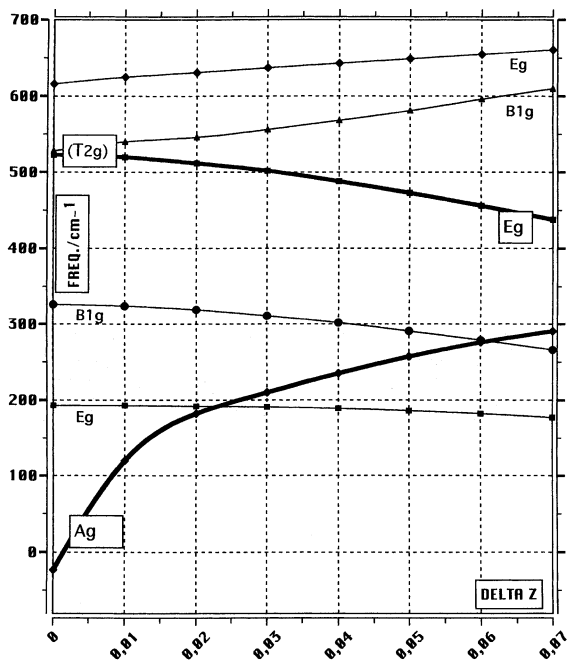

Fig. 6. Raman active frequencies of t-ZrO$_2$ as a function of the Δz value for the PQ2 crystal with nominal Δz value at 0.0047. Bold curves represent the evolution of the two phonon frequencies discussed in this paper.

mentally observed frequency shifts can be readily revealed: t-ZrO_2 structure existing at RT in the metal/oxide interface has a high internal tetragonality i.e., the Δz value in this structure is higher than in 'ordinary' powder-like samples ('super-tetragonality').

To clarify more deeply the nature of the above dependences of the phonon frequencies on the Δz value magnitude, we decided to answer the question: how all the Raman spectrum of t-ZrO_2 would change when Δz value vary from 0 up to 0.070. The results of this study are shown in Fig. 6. These clearly exhibit that the phonon having frequency 267 cm^{-1} in the ordinary t-ZrO_2 lattice softens drastically when Δz diminishes, and vanishes at $\Delta z = 0$. Obviously, this is the soft mode responsible for the c–t phase transition. In parallel, the phonon having the frequency near 456 cm^{-1} in ordinary t-ZrO_2 lattice hardens and, in merging together with another phonon at $\Delta z = 0$, becomes the T_{2g} Raman active mode of cubic ZrO_2 (see Fig. 6). Below the transition point, the internal tetragonal deformation Δz splits the T_{2g} phonon frequency into the $E_g + B_{1g}$ doublet so that the vibration having position 456 cm^{-1} in t-ZrO_2 is the lower-frequency E_g component of the doublet. This E_g component would decrease in t-phase, whereas the soft-mode frequency would increase. That is why the Δz-dependences of the above two vibrations A_{1g} and E_g have different signs.

The cohesive energy (CE) per unit formula ZrO_2, nearly 24 eV [27,28], changes with the increase of internal tetragonality. This change can be estimated from an ab initio CE calculation [27]. The t–c change in a classical graph of the CE vs Δz corresponds to a passage from a double well-structure to a quasi-simple one [27,29,30]. In the tetragonal phase, the oxygen atom vibrates in one of the two deep potential wells and in the cubic phase the oxygen atom is instable and oscillates in a quasi-plane large simple well. This t–c phase change needs a 80 meV CE change, associated particularly with the lowering of the double barrier, the shortening of Δz to zero, and the modifications of a/c to unity. This result is in correct agreement with other experimental or theoretical values [31] and is consistent with the thermodynamic energy $k\Delta T$ (86 meV) for the ΔT increase needed in the t–c transformation. In our simulation the increase of Δz value which well represents the observed shifts of frequencies, is only +15% of the total Δz variation in the t–c phase change, it would correspond to a variation of CE of 10 meV.

6. Conclusion

Our study reveals the lattice-dynamical (structural) source of the frequency shifts displayed by the modes near 282 and 443 cm^{-1} in the t-ZrO_2 lattices existing in the metal/oxide interface [1]. It is highly likely, that this phenomenon comes from the 'super-tetragonality' of this lattice. We believe, that this conclusion is in line with the experimental effects recently observed by Bouvier and Lucazeau [18,32], whatever the mode assignment would be. It is shown in [18,32] that hydrostatic compression would transform the tetragonal ZrO_2 lattice, $\Delta z = 0.045\ c$, into the cubic one ($\Delta z \rightarrow 0$), so that the mode with the frequency at 267 cm^{-1} would finally vanish, whereas the mode with the frequency at 456 cm^{-1} would harden. In other words, it follows from [18,32] that $\partial(267\ \mathrm{cm}^{-1})/\partial z > 0$ and $\partial(456\ \mathrm{cm}^{-1})/\partial z < 0$; our calculations show the same result. This makes it evident that the 'abnormally' high value of the oxygen displacement Δz from its position in c-ZrO_2 lattice is indeed responsible for the *hardening* of the mode normally situated near 267 cm^{-1}, and for the *softening* of the mode normally situated near 456 cm^{-1}. This conclusion on the 'super-tetragonality' of t-ZrO_2 in oxide films is not, of course, inconsistent with the well established compressive stresses at the metal/oxide interface. However, according to our results those stresses cannot explain the frequency shifts under consideration (Section 1). The frequency shifts that these stresses would induce must yet superpose upon those of Δz displacement but this last one is finally preponderant in the explanation of the Raman frequency shifts already observed [1].

The calculation unequivocally shows that these two modes, 267 and 456 cm^{-1}, have A_{1g} and E_g symmetry respectively, thus clarifying the important problem of the position of the totally symmetric A_{1g} mode in the Raman spectra of t-ZrO_2 [22–24,33] which cannot be a mode with a frequency near 600 cm^{-1} as it is widely accepted in the literature. Let us note that our assignment of the mode 267 cm^{-1} (A_{1g}) is in full correspondence with the reliable experimental results obtained from the polarized Raman scattering of the bulk crystals of t-ZrO_2 [24]. It is worthy noting that this is not inconsistent with the recent experimental results [18] obtained for pressure dependence of t-ZrO_2 Raman frequencies, which show an anti-crossing effect between the curves corresponding to the 267 cm^{-1} and the lower frequency band. Let us recall that non-interacting lattice waves 'exist' in the harmonic theory only, and the presence of the anharmonic terms makes these waves to form the bounded states (see e.g., [36], Section 65). Thus, strictly speaking, the anti-crossing effect would always exist (more or less strong) in practice, as a consequence of (i) the anharmonicity of the real crystal, (ii) the structural defects violating the symmetry selection rules, what can be quite reasonably expected for the nanometric powder used in [18]. Anti-crossing effect cannot be a definitive proof of the same symmetry of the interacting waves.

The internal tetragonality with extremely high Δz value ('super-tetragonality') needs a 10 meV increase of

CE and can be linked to a more sub-stoechiometric t-ZrO_2 structure ([1,34,35] and references therein). Moreover, it is well known that the absence of stabilizing factors, like additive oxides, increases Δz value [15].

References

[1] P. Barbéris, T. Merle, P. Quintard, J. Nucl. Mater. 246 (1997) 232.

[2] Y.P. Lin, O.T. Woo, D.J. Lockwood, Mater. Res. Soc. Symp. Proc. 343 (1994) 487.

[3] O.T. Wood, D.J. Lockwood, Y.P. Lin, V.F. Urbani, Mater. Res. Soc. Symp. Proc. 357 (1995) 219.

[4] M.B. Smirnov, A.P. Mirgorodsky, P.E. Quintard, J. Molec. Struct. 348 (1995) 159.

[5] A.P. Mirgorodsky, M.B. Smirnov, P.E. Quintard, J. Phys. Chem. Solids 60 (1999) 985.

[6] G. Teufer, Acta Crystallogr. 15 (1982) 1187.

[7] P. Aldebert, J.P. Traverse, J. Am. Ceram. Soc. 68 (1985) 34.

[8] N. Igawa, Y. Ishii, T. Nagasaki, Y. Morii, S. Funahashi, J. Am. Ceram. Soc. 76 (1993) 2673.

[9] E. Djurado, E. Meunier, J. Solid State Chem. 140 (1998) 191.

[10] M.C. Silva, thèse, Université de Limoges, 1996.

[11] C.J. Howard, B.A. Hunter, D.-J. Kim, J. Am. Ceram. Soc. 81 (1998) 241.

[12] H.G. Scott, J. Mater. Sci. 10 (1975) 1527.

[13] H. Toraya, J. Am. Ceram. Soc. 72 (1989) 662.

[14] M. Yashima, H. Arashi, M. Kakihana, M. Yoshimura, J. Am. Ceram. Soc. 77 (1994) 1067.

[15] E.H. Kisi, C.J. Howard, in: Zirconia Engineering Ceramics-Old Challenges, New Ideas, vol. 153&154, TransTech, Zurich, 1998, p. 1.

[16] H.J. Beie, A. Mitwalsky, F. Garzarolli, H. Ruhmann, H.G. Sell, ASTM-STP 1245 (1994) 615.

[17] N. Petigry, P. Barbéris, C. Lemaignon, Ch. Valot, M. Lallemant, J. Nucl. Mater. 280 (2000) 318.

[18] P. Bouvier, G. Lucazeau, J. Phys. Chem. Solids 61 (2000) 569.

[19] D. Michel, M.T. Van Den Borre, A. Ennaciri, Advances in Ceramics, vol. 24, Science and Technology of Zirconia III, American Ceramic Society, 1988, p. 555.

[20] C. Valot, thèse, Université de Bourgogne, 1995.

[21] A.P. Mirgorodsky, M.I. Baraton, P.E. Quintard, J. Phys.: Condens. Matter 1 (1989) 10053.

[22] A.P. Mirgorodsky, M.B. Smirnov, P.E. Quintard, J. Phys. Chem. Solids 60 (1999) 985.

[23] P.E. Quintard, P. Barbéris, A.P. Mirgorodsky, T. Merle, J. Am. Ceram. Soc., to be published.

[24] Yu.K. Voronko, M.A. Zufarov, B.V. Ignatev, V.V. Osiko, E.E. Lomonova, A.A. Sobol, Opt. Spectrosc. 51 (4) (1981) 315.

[25] A.P. Mirgorodsky, M.B. Smirnov, T. Merle, P. Quintard, J. Mater. Sci. 34 (1999) 4845.

[26] A.P. Mirgorodsky, P.E. Quintard, J. Am. Ceram. Soc. 82 (1999) 3121.

[27] G. Jomard, T. Petit, A. Pasturel, L. Magnaud, G. Kresse, J. Hafner, Phys. Rev. B 59 (1999) 4044.

[28] A. Christensen, E.A. Carter, Phys. Rev. B 58 (1998) 8050.

[29] R. Orlando, C. Pisani, C. Roetti, E. Stefanovitch, Phys. Rev. B 45 (1992) 592.

[30] M. Wilson, U. Schonberg, M.X. Finnis, Phys. Rev. B 54 (13) (1996) 9147.

[31] H.J.F. Jansen, Phys. Rev. B 43 (1991) 7267.

[32] P. Bouvier, G. Lucazeau, private communication.

[33] N. Kjerulf-Jensen, R.W. Berg, F.W. Poulsen, in: Proceedings of the Second European Solide-Oxide Fuel Cell Forum, vol. 2, Oslo, 1996, p. 647.

[34] Waterside corrosion of zirconium alloys in nuclear power plants, IAEA-Techdoc 996, Jan. 1998, p. 254.

[35] H. Tomaszewski, K. Godwood, J. Europ. Ceram. Soc. 15 (1995) 17.

[36] L. Landau, E. Lifchitz, Physique Statistique, vol. 5, Mir, Moscou, 1967.